Spin lifetime of donor and conduction band states in n-type GaAs at the metal-insulator transition

L. Schreiber, M. Heidkamp, T. Rohleder, B. Beschoten,* and G. Güntherodt
II. Physikalisches Institut, and Virtual Institute for Spin Electronics (ViSel), RWTH Aachen University, Templergraben 55, 52056 Aachen, Germany
(Dated: May 20, 2007)

The energy dependence of electron spin lifetimes is investigated in n-type GaAs near the metal-insulator transition by time-resolved Kerr rotation. The spin lifetimes vary by three orders of magnitude as a function of energy when occupying donor and conduction band states. For delocalized donor band states we find the longest spin lifetimes, which exhibit a strong reduction in a transverse magnetic field. The occupation of localized donor band states is identified by a reduced spin lifetime and a distinct Overhauser shift due to dynamic nuclear polarization. The energies of the pump and probe laser are tuned independently to allow for cooling of excited hot electron spins.

PACS numbers: 78.47.+p, 78.55.Cr, 85.75.-d

Within the framework of the emerging field of spintronics, the spin degree of freedom is exploited for information storage and processing and could serve as a qubit for quantum computation [1]. Spin coherence and long spin lifetimes are a prerequisite for novel spintronic devices. Electron spins in Si-doped bulk n-GaAs drew attention, when long spin lifetimes $T_2^* > 100$ ns and coherence lengths larger than 100 μm were determined using time-resolved Faraday rotation [2, 3]. Since then n-GaAs was used as a model system to investigate spin injection and spin transport phenomena [4–6]. In this regard, at low temperatures bulk n-GaAs is superior to low-dimensional III/V systems, since it offers itinerant spins exhibiting long T_2^* and thus allows spatio-temporal studies of coherent spin transport. In contrast, T_2^* of spins in two-dimensional zinc-blende semiconductor heterostructures often suffers from the enhanced efficiency of the D'yakonov-Perel' (DP) dephasing [7] or exhibits anisotropic spin scattering [8, 9].

The long T_2^* of bulk n-GaAs, however, is restricted to a doping concentration in the vicinity of the metal-insulator transition (MIT) and shortens dramatically towards both sides of the transition [2, 10]. Similar results in n-type GaN [11], and n-type Si [12] point to a universal phenomenon. In n-GaAs, various spin relaxation mechanisms have been considered to explain the dependence of T_2^* upon carrier concentration, temperature and transverse magnetic field B. The relevant relaxation mechanisms differ substantially for delocalized spins with, e.g., the DP dephasing mechanism [13–16], and for spins localized at impurity sites with, e.g., relaxation by hyperfine interaction [16–18]. The MIT in n-type semiconductors takes place within the donor band (DB) [19], which is well-separated from the conduction band (CB). The electronic structure near the Fermi energy (E_F) is governed by both doping induced disorder and local Coulomb correlation. The former yields Anderson-localized states in the upper and lower donor band-tails, which are separated from extended states in the center by mobility edges [20]. The latter may lead to a Coulomb gap U at E_F [21]. Both interactions yield a complex electronic structure with coexisting localized and delocalized DB states as well as CB states. Spin dephasing in n-GaAs has mostly been investigated for states at E_F [2, 3]. There is, however, no study of T_2^* spanning the whole energy range of DB and CB states.

In this Letter, we study the spin lifetime T_2^* of coherent electron spin states in n-GaAs, which are optically excited in both the donor and conduction band and probed by time-resolved Kerr rotation (TRKR) at 6 K. Due to the coexistence of distinct electronic states, the sample is not characterized by a single T_2^*: T_2^* varies by three orders of magnitude as a function of photon energy. The longest T_2^* values are found for delocalized donor band states, while free conduction band states exhibit shorter spin lifetimes. Our time-resolved Kerr signal shows up to three exponential decay regimes with different precession frequencies. The latter can change due to an additional nuclear magnetic field arising from dynamically polarized nuclei, when resonantly pumping spins into localized DB states.

Two (001)-oriented, 500 μm thick GaAs wafers with different Si-doping concentrations have been investigated: Sample A with a carrier concentration of $(2.4 \pm 0.2) \times 10^{16}$ cm^{-3} is doped close to the MIT (critical carrier concentration in Si:GaAs $n_c \cong 1.5 \times 10^{16}$ cm^{-3}) [19]. Reference sample B has a carrier concentration of $(1.5 \pm 0.4) \times 10^{18}$ cm^{-3} and is therefore degenerated [21]. We used two tuneable, mode-locked Ti:Al_2O_3 lasers providing ~150 fs optical pulses corresponding to a spectral width of $\approx$ 6 nm at a repetition frequency of 80 MHz. Electronic phase-locking of both lasers enables us to employ one laser for spin pumping at an energy E_{pu} and the other one for probing the spin orientation at an energy E_{pr} after a variable delay time $\Delta t = 0...16$ ns. The normal-incident pump pulses, which were circularly polarized by a photo-elastic modulator (PEM), excite spin-polarized electrons and holes oriented along the beam

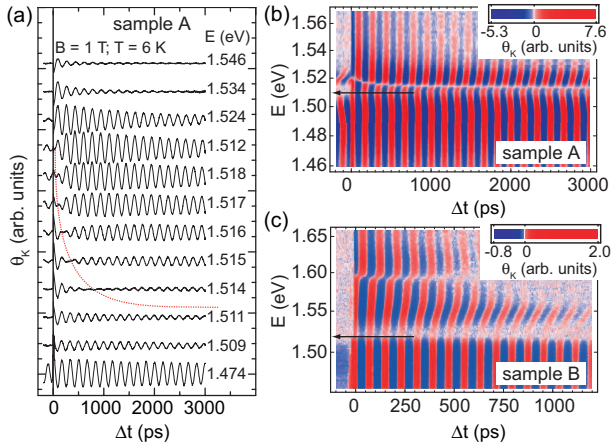

FIG. 1: (Color) Time-resolved Kerr rotation for photon energies $E = E_{pu} = E_{pr}$ at 6 K with (a) $\theta_K(\Delta t)$ for sample A at $B = 1$ T; the red line shows the shift of the beating node; (b) $\theta_K(\Delta t, E)$ for sample A at $B = 1$ T; (c) $\theta_K(\Delta t, E)$ for the degenerate sample B at $B = 6$ T. Arrows mark the respective energies, above which the transmission drops below 5%.

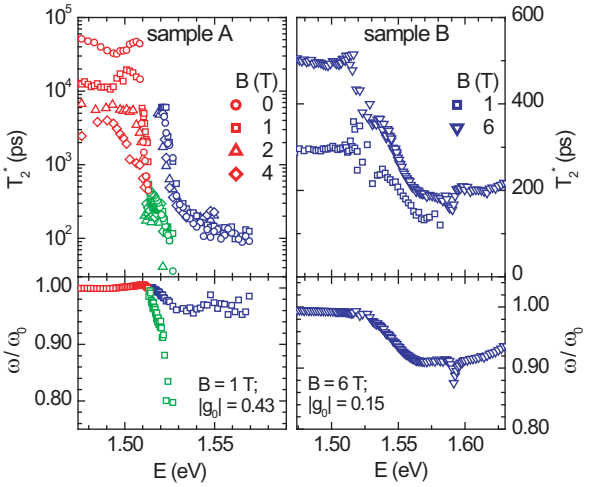

FIG. 2: (Color) Fitted spin lifetimes $T_2^{*(i)}$ and Larmor frequencies $\omega^{(i)}$ as a function of photon energy $E = E_{pu} = E_{pr}$ for MIT sample A (left) and degenerate sample B (right) at various magnetic fields B. The colors mark three energy regions as discussed in the text. The Larmor frequencies are normalized to ω_0 calculated from $|g_0| = 0.43$ and $|g_0| = 0.15$ for sample A and B, respectively.

direction in the strain-free mounted samples with an average power $\langle P \rangle = 50$ W/cm^2. The projection of the pump induced spin magnetization onto the surface normal of the sample is determined with linearly polarized laser pulses by Faraday rotation θ_F in transmission and by Kerr rotation θ_K in reflection. Transverse magnetic fields B are applied in the plane of the sample.

In Figure 1(a), we plot $\theta_K(\Delta t)$ of sample A measured for various photon energies $E = E_{pu} = E_{pr}$ at $B = 1$ T and at $T = 6$ K. Obviously, the spins precess at all energies E, but the damping of the oscillations and thus T_2^* is E-dependent: for E below the CB edge T_2^* is long, whereas for the highest E, at which CB states are pumped, T_2^* is much reduced. Strikingly, a node in the oscillation envelope (red line in Fig. 1(a)) near the band edge indicates that the spins precess with at least two Larmor frequencies $\omega^{(i)}$. Therefore, $\theta_K(\Delta t)$ is described by n decay components

$$\theta_K(\Delta t) = \sum_i^n A^{(i)} \exp\left(-\frac{\Delta t}{T_2^{*(i)}}\right) \cos\left(\omega^{(i)} \Delta t + \phi^{(i)}\right), \quad (1)$$

where $A^{(i)}$, $T_2^{*(i)}$ and $\phi^{(i)}$ are the initial amplitude, the spin lifetime and the phase of component i, respectively. Since this beating node shifts with increasing E towards $\Delta t = 0$, the difference of the two $\omega^{(i)}$ increases. The Larmor frequencies $\omega^{(i)} = g^{*(i)} \mu_B B/\hbar$ depend upon component-specific effective g-factors $g^{*(i)}$. Note that the pump-induced spin packets, which exhibit a *continuous* distribution of g-factors, precess with only one energetically averaged g^* but with reduced T_2^* due to inhomogeneous dephasing [2]. Thus, electronic states with two g-factor dispersions like, e.g., DB and CB states are pumped simultaneously to yield separated $\omega^{(i)}$. Figure 1(b) displays $\theta_K(\Delta t, E)$ of sample A in a false color plot. The E-dependence of $\omega^{(i)}$ is obvious from horizontal drifts of maxima and minima of θ_K and most distinct at the band edge (horizontal arrow). Non-vanishing θ_K at $\Delta t < 0$ evidence long $T_2^* \gtrsim 6$ ns, since the signal stems from spins exited by the previous pump pulse. In Figure 1(c), this result is compared to $\theta_K(\Delta t, E)$ of the degenerate sample B, for which E_F lies well within the CB. For this sample, both T_2^* and g^* depend strongly on E in the absorbing energy regime. However, there are no nodes in the oscillation envelope at any energy. Note that the identity of DB states is completely lost in this degenerate sample. This indicates that the multi-component decay as well as the nodes in the oscillation amplitude of sample A may arise from distinct DB and CB states.

To further support these findings, we plot in Figure 2 both $T_2^{*(i)}(E)$ and $\omega^{(i)}(E)$ values as determined from least-squares fits of $\theta_K(\Delta t, E)$ according to Eq. 1 for both samples and for various B fields. The values of long $T_2^* > 20$ ns observed at $B = 0$ T are extracted from fits of resonant spin amplification scans [2]. For sample A, T_2^* drops by more than 3 orders of magnitude as a function of photon energy E, however, three energy regions can be distinguished marked by red, green and blue symbols. At low E (red), T_2^* is nearly independent of E but decreases rapidly with the increase of B. In this regime we also observe $T_2^* \approx 110$ ns at $B = 0$ T at reduced pump power $\langle P \rangle = 10$ W/cm^2 (not shown) similar to Ref. [2]. Approaching the CB edge T_2^* drops at all B,

but the Larmor frequency for the whole range is almost constant and exhibits $|g^*| = |g_0| = 0.43$. Near the CB edge (green), B-independent values of $T_2^* \sim 100...300$ ps are determined, which distinguish themselves by a rapid decrease of $\omega(E)$. At the beginning of the third region (blue), T_2^* sets-in at ~ 6 ns and decreases with increasing E. The corresponding ω decreases slightly and saturates at high E. The overlap of the second and third region, which is enhanced by the spectral width of the laser pulses, generates the node in the oscillation envelope shown in Figure 1 [22]. For the degenerate sample B, $T_2^{*(i)}(E)$ can be fitted by one component i. As expected [2, 10], T_2^* is over-all shorter compared to sample A and T_2^* increases with the increase of B, which is typical for the DP dephasing mechanism [13].

In the following, we assign the $T_2^{*(i)}$ of the spins observed in the three energy ranges to carriers occupying different electronic states. Since hole spins relax quickly $\lesssim 10$ ps in GaAs and excitons are broken up at high magnetic fields $B \gtrsim 1$ T [23], we consider single electron states. Since the carrier concentration of sample A is slightly above n_c, E_F lies within the delocalized DB states as sketched in Figure 3. Thus delocalized DB states are pumped at lowest E, which exhibit the longest T_2^* (red component in Fig. 2). However, to our knowledge there is no relaxation mechanism of spins, which accounts for their distinct B-dependence. We assign the second energy range (green), which is missing for the degenerate sample B, to Anderson localized electronic states at the DB tail. Their distinct E-dependence of ω and T_2^* can be linked to the decrease of localization length upon approaching the DB tail. The localization of electrons yields spin relaxation due to hyperfine interaction with the nuclei [17, 18]. This gives rise to dynamic nuclear polarization and a nuclear field, which alters ω (Overhauser shift) [24]. However, from Ref. [17] long $T_2^* \sim 300$ ns are expected for localized electron spins, although we could not reproduce this result with insulating n-GaAs samples using TRKR. In Ref. [18], an additional short $T_2^* \sim 100$ ps component is predicted, when both localized and delocalized spins are pumped. This is assigned to their cross-relaxation rate. Whereas this might explain our short T_2^*, it does not account for the distinct $\omega(E)$ dependence. In the third energy regime (blue), electrons are pumped in the CB. The decrease of ω observed for both samples is due to g^*: The absorption of the pump pulse lifts the local chemical potential, thus reducing the absolute value of the energetically averaged g^* factor according to its dispersion in the CB [23]. The apparent decrease of $T_2^*(E)$ might be explained by carrier cooling and interband relaxation. Due to both, the carriers relax below the probed energy.

This notion can be confirmed by sweeping E_{pu} with E_{pr} held fixed at the bottom of the CB. The corresponding fits of $T_2^{*(i)}(E_{pu})$ and $\omega^{(i)}(E_{pu})$ of sample A

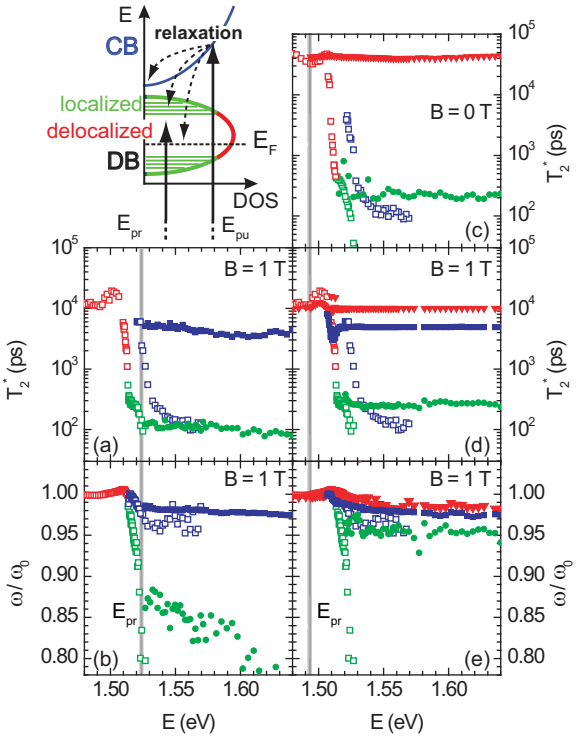

FIG. 3: (Color) Upper left: sketch of density of DB and CB states. Fitted spin lifetimes $T_2^{*(i)}$ and Larmor frequencies $\omega^{(i)}$ as a function of pump laser energy E_{pu} at magnetic fields B for MIT sample A (filled symbols) for different probe energies E_{pr} is marked with vertical grey lines. For comparison data from Fig. 2 with $E_{pu} = E_{pr}$ are also plotted (open symbols).

at $B = 1$ T are shown in Figure 3(a) and (b). Indeed, this method allows to correct T_2^* for energy relaxation, since $T_2^*(E_{pu})$ (blue full symbols) decreases only slightly compared to Figure 2. However, there is an additional short $T_2^{*(i)}(E_{pu})$ (green full symbols), which results from probing localized spins at the DB tail because of the spectral width of the probe pulses. To clarify this point, E_{pr} is fixed at an energy even lower than the band gap (Fig. 3(c)-(e)). For this E_{pr}, the longest $T_2^{*(i)}(E_{pu})$ (red) attributed to delocalized DB states is observed, which turned out to be nearly constant at $B = 0$ T. Note that the average pump power is held constant, but the excited carrier density changes by orders of magnitude in the absorbing regime. This has a negligible effect on the longest T_2^*. More strikingly, additional components i become observable, when E_{pu} passes the localized and CB states. Thus, different electronic states become occupied either due to direct optical excitation or carrier relaxation as sketched in Figure 3(upper left). From the onset of the θ_F signal (not shown), we deduce that the delocalized DB states are occupied within $\Delta t < 10$ ps for all E_{pu}. At $B = 1$ T (Fig. 3(d)) and E_{pu} beyond the band edge, the two long $T_2^{*(i)}$ components (blue and red) generate nodes in the oscillation envelope (Fig. 1(a)) and can be

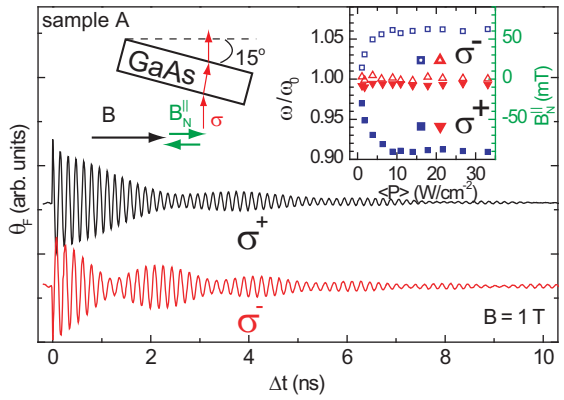

FIG. 4: (Color) Faraday rotation $\theta_F(\Delta t)$ of sample A for left (σ^-) and right (σ^+) circularly polarized pump pulses (red arrows) at $B = 1$ T, $E_{pu} = 1.514$ eV and $E_{pr} = 1.494$ eV. Inset: fitted normalized Larmor frequencies $\omega^{(i)}$ and corresponding lateral nuclear magnetic fields $B_N^{\parallel}$ for both polarizations as a function of the average pump power.

separated by their $\omega^{(i)}$ (Fig. 3(e)). For fitting, however, the longest T_2^* (red) of delocalized DB had to be fixed with minor influence on the blue component. The latter can be clearly assigned to CB states by comparing it to $T_2^*(E_{pu})$ and $g^*(E_{pu})$ of Figure 3(a) and (b). The existence of three components i and their onset when sweeping E_{pu} confirms our assignment of $T_2^{*(i)(E)}$ to the three types of electronic states.

Since an optically pumped spin imbalance of localized electrons leads to pronounced dynamic nuclear polarization (DNP) [24], we finally check our assignment of electronic states to T_2^* by identifying DNP. When resonantly exciting localized spins at, e.g., $E_{pu} = 1.514$ eV, then DNP is optically observed by the Overhauser shift. This shift results in a change of ω due to the presence of a lateral nuclear magnetic field $B_N^{\parallel}$ adding up to B. Since spins exhibiting long T_2^* are most sensitive to this shift, we chose the same E_{pr} as in Figure 3(c)-(e). In order to generate a well-defined longitudinally pumped spin component and thus to control the direction of $B_N^{\parallel}$ with respect to B, we replaced the PEM by a quarter-waveplate and rotated sample A as sketched in Figure 4 [25]. In this geometry, $\theta_F(\Delta t)$ exhibits nodes in the oscillation envelope at long Δt, proofing the presence of two long $T_2^{*(i)}$ components with different $\omega^{(i)}$. The dependence of ω on the type of circularly polarization $\sigma^{\pm}$ of the pump pulses, is clarified by the fitted $\omega^{(i)}$ in the inset of Figure 4. The sign and magnitude of $B_N^{\parallel}$ is determined by $\sigma^{\pm}$ and the pump power, respectively. $B_N^{\parallel}$ saturates for σ^+ at -90 mT, when $|g^*| = 0.43$ is assumed to be constant. However, the blue component, which is likely due to spins in the CB (cp. to Fig. 3(e)), is more sensitive to B_N than the spins attributed to delocalized DB states (red). However, this point needs further investigation. Since DNP is not observable when E_{pu} is reduced below 1.5 eV, our assignment of localized states is confirmed. The pronounced $\omega(E)$ dependence of the localized spins (green) (see Fig. 2 left) compared to the variation of ω in the inset of Figure 4 suggests that this $\omega(E)$ is indeed influenced by increasing localization and thus responsible for a rise of $B_N^{\parallel}$ at the DB tail [26].

In conclusion, we have attributed the complex photon energy dependence of the electron spin lifetimes in n-type GaAs to energy relaxation and to occupation of conduction band, delocalized and localized donor band states. The longest lifetimes are found for delocalized donor band states, whereas localized spins relax rather fast. Resonant pumping of the localized donor band states yields strong dynamic nuclear polarization.

This work was supported by BMBF and by HGF.

* Electronic address: beschoten@physik.rwth-aachen.de

[1] D. D. Awschalom and M. E. Flatte, Nature Phys. **3**, 153 (2007).
[2] J. M. Kikkawa and D. D. Awschalom, Phys. Rev. Lett. **80**, 4313 (1998).
[3] J. M. Kikkawa and D. D. Awschalom, Nature **397**, 139 (1999).
[4] Y. Kato *et al.*, Science **306**, 1910 (2004).
[5] S. A. Crooker *et al.*, Science **309**, 2191 (2005).
[6] X. Lou *et al.*, Nature Phys. **3**, 197 (2007).
[7] M. I. D'yakonov and K. V. Yu, Fiz. Tekh. Poluprovodn. (Leningrad) **20**, 178 (1986).
[8] S. Döhrmann *et al.*, Phys. Rev. Lett. **93**, 147405 (2004).
[9] L. Schreiber *et al.*, Phys. Rev. B **75**, 193304 (2007).
[10] R. I. Dzhioev *et al.*, Phys. Rev. B **66**, 245204 (2002).
[11] B. Beschoten *et al.*, Phys. Rev. B **63**, 121202 (2001).
[12] V. Zarifis and T. G. Castner, Phys. Rev. B **36**, 6198 (1987).
[13] J. Fabian and S. Das Sarma, J. Vac. Sci. Technol. B **17**, 1708 (1999).
[14] P. H. Song and K. W. Kim, Phys. Rev. B **66**, 035207 (2002).
[15] Z. G. Yu and S. Krishnamurthy, Phys. Rev. B **71**, 245312 (2005).
[16] B. I. Shklovskii, Phys. Rev. B **73**, 193201 (2006).
[17] R. I. Dzhioev *et al.*, JETP Lett. **74**, 200 (2001).
[18] W. O. Putikka and R. Joynt, Phys. Rev. B **70**, 113201 (2004).
[19] D. Romero *et al.*, Phys. Rev. B **42**, 3179 (1990).
[20] P. Anderson, Phys. Rev. **189**, 1492 (1958).
[21] A. Efros and M. Pollak, eds., *Electron-Electron Interaction in Disordered Systems* (North-Holland, Amsterdam, 1984).
[22] The third region sets in at even lower energy $E \approx 1.514$ eV, where T_2^* cannot be determined exactly due to the beating.
[23] M. Oestreich *et al.*, Phys. Rev. B **53**, 7911 (1996).
[24] D. Paget *et al.*, Phys. Rev. B **15**, 5780 (1977).
[25] G. Salis *et al.*, Phys. Rev. B **64**, 195304 (2001).
[26] Even with the PEM, we observe drifts of ω after switching on the pump. We attribute this to an Overhauser shift.